miR-17-5p Inhibits BNIP3-Mediated Mitochondrial Autophagy to Attenuate Pathological Cardiac Fibrosis

Derong Huang, Qing Wen, Yuchen Su, Xiumao Li

Department of Cardiovascular Surgery, Affiliated Hospital of Zunyi Medical University, Guizhou, China

Background: Cardiac fibrosis plays a critical role in the progression of chronic cardiovascular conditions, with mitochondrial dysfunction acting as a central mechanism underlying pathological myocardial fibrosis. Increasing research shows that microRNAs may modulate the fibrotic process by regulating mitochondrial function via various pathways.

Aims: To examine the involvement of miR-17-5p in modulating mitochondrial autophagy and alleviating pathological cardiac fibrosis.

Study Design: Combined *in vivo* and *in vitro* study.

Methods: Expression levels of miR-17-5P and BCL2/adenovirus E1B 19 kDa protein-interacting protein 3 (BNIP3) were measured in a mouse model of myocardial fibrosis induced by abdominal aortic constriction, as well as in cardiac fibroblasts (CFs) treated with angiotensin II. CFs were transiently transfected with a miR-17-5p mimic, the pcDNA3.1-BNIP3 plasmid, or both. Cell viability was evaluated using the CCK-8 colorimetric assay. The expression of fibrotic and autophagy-related markers was determined via quantitative real-time reverse transcription polymerase chain reaction and immunoblotting. Intracellular levels of reactive oxygen species (ROS) and adenosine triphosphate (ATP) were also assessed.

Results: Reduced myocardial miR-17-5p expression was associated with diminished left ventricular systolic function and increased collagen accumulation in heart tissue. *In vitro*, angiotensin II treatment led to decreased miR-17-5p expression, upregulated BNIP3, and excessive mitochondrial autophagy-evidenced by increased ROS, lowered ATP production, and elevated fibrosis-related markers. Rescue experiments demonstrated that miR-17-5p overexpression directly targeted the 3' untranslated region (3'-UTR) of BNIP3, significantly downregulating its expression, restoring mitochondrial balance, and decreasing collagen production. Conversely, BNIP3 overexpression counteracted the anti-fibrotic and mitochondrial-protective effects of miR-17-5p.

Conclusion: The miR-17-5p/BNIP3 signaling pathway modulates mitochondrial autophagy in CFs and plays a key role in fibrotic remodeling. This axis may serve as a promising therapeutic target for reducing cardiac fibrosis and slowing the progression of heart failure.

INTRODUCTION

Cardiovascular diseases remain a significant global public health burden, responsible for 31% of all deaths worldwide.[1,2] Cardiac fibrosis-a hallmark of heart failure-is commonly observed in conditions such as hypertensive heart disease, dilated cardiomyopathy, and myocardial degeneration associated with aging.[3] This pathological process is characterized by an abnormal accumulation of fibrillar collagen and other extracellular matrix (ECM) components within the myocardial interstitium, resulting in increased myocardial stiffness, decreased ventricular compliance, and ultimately, maladaptive ventricular remodeling and progressive cardiac dysfunction.[4,5]

Cardiac fibrogenesis involves complex interactions among various dysregulated signaling pathways, including those associated with inflammation, oxidative stress, and regulated cell death mechanisms such as autophagy and apoptosis.[6] Mitochondria play a central role in this process, serving as key regulators of cellular energy metabolism and redox homeostasis. Under pathological conditions, mitochondrial structural integrity becomes compromised, leading to elevated production of reactive oxygen species (ROS) and disturbances in mitochondrial dynamics. The accumulation of ROS further aggravates mitochondrial injury, perpetuating a cycle of cellular dysfunction. For example, exposure to particulate matter 2.5 has been found to trigger aortic fibrosis via the PINK1/Parkin-mediated mitophagy[7], while excessive mitochondrial oxidative phosphorylation activity enhances fibroblast activation and ECM remodeling.[8]

MicroRNAs (miRNAs) modulate gene expression by binding in a sequence-specific manner to epitopes in the 3'-UTR of target mRNAs, thereby repressing gene repression at the post-transcriptional level.

Several miRNAs have been associated with the regulation of cardiac fibrosis. miR-17-5p is involved in various pathological conditions. In neurological diseases, miR-17-5p alleviates ischemic brain damage by inhibiting neuroinflammatory responses[9], and in metabolic disorders, it facilitates diabetic wound healing by improving endothelial cell function.[10] In addition, miR-17-5p has been reported to protect fibroblasts by modulating neutrophil extracellular trap formation[11]; however, its specific role in the development of cardiac fibrosis remains inadequately defined.

BCL2/adenovirus E1B 19 kDa protein-interacting protein 3 (BNIP3), a critical autophagy-related protein, regulates fibrosis in multiple organs via mitophagy. In renal fibrosis, BNIP3 activity is influenced by the vitamin D receptor, which helps correct autophagy in diabetic mice and modulates streptozotocin-induced kidney fibrosis.[12] The HIF1α-BNIP3 axis promotes mitophagy, thereby reducing hypoxia-induced damage in renal epithelial cells and limiting fibrogenesis through the elimination of mitochondrial ROS and inhibition of NLRP3 inflammasome activation.[13] In liver fibrosis, BNIP3 expression is elevated in fibrotic liver tissue and activated hepatic stellate cells, while its suppression reduces stellate cell activation and fibrosis severity.[14] In lung fibrosis, BNIP3 expression levels are associated with clinical outcomes in idiopathic pulmonary fibrosis, highlighting its potential as a therapeutic target.[15] Additionally, mutations in FBXL4 lead to abnormal BNIP3/BNIP3L accumulation, excessive mitophagy, and mitochondrial DNA depletion syndrome; silencing BNIP3/BNIP3L reverses fibrotic changes across multiple organs.[16] Although BNIP3-driven mitophagy has been strongly linked to fibrosis, its specific role in myocardial fibrosis remains insufficiently understood.

This study elucidates the molecular mechanism by which miR-17-5p contributes to myocardial fibrosis, utilizing both mouse models of cardiac fibrosis and cardiac fibroblasts (CFs). We further delineated the signaling cascade regulated by the miR-17-5p/BNIP3 axis that affects pathological myocardial fibrosis by modulating mitochondrial autophagy. Moreover, we conducted an in-depth investigation into the regulatory pathways connecting the miR-17-5p/BNIP3 axis, mitophagy, and CF function. The findings demonstrate that this axis plays a role in CF activation and collagen deposition by maintaining mitochondrial homeostasis, thereby highlighting a potential new therapeutic approach for treating fibrosis.

MATERIALS AND METHODS

Experimental animals

All experimental procedures were reviewed and the study was approved by the Animal Ethics Committee of Zunyi Medical University (approval number: zyfy-an2023-0152, date: 26.12.2023). Wild-type (WT) male C57BL/6J mice (6-8 weeks old, 20-25 g) were randomly assigned to either the sham or abdominal aortic constriction (AAC) group (n = 6 per group). The sample size was determined based on previously published studies involving murine models of cardiac disease.[4,17] Mice were housed individually in specific pathogen free-grade cages under controlled conditions (temperature 22 °C-26 °C, relative humidity 50%-70%) with a 12-hour light/dark cycle. For the surgical procedure, mice in the AAC group were anesthetized with 2% isoflurane, after which a midline abdominal incision was made to expose the abdominal aorta. A constriction was then applied to produce a standardized narrowing of 0.6 mm. Sham-operated mice underwent the same surgical steps without aortic ligation. Echocardiographic evaluations were conducted at 4, 8, and 12 weeks following surgery. After the final imaging session, body weight (g) was recorded, mice were euthanized using an overdose of anesthesia, and the hearts were immediately excised for wet weight measurement (mg). Left ventricular (LV) myocardial tissues were collected either by snap-freezing in liquid nitrogen or by paraffin embedding for subsequent analyses.

Echocardiographic measurements

Mice were anesthetized using isoflurane inhalation and positioned in sternal recumbency on a temperature-controlled platform. The following cardiac parameters were measured: LV ejection fraction, end-diastolic diameter, end-systolic diameter, and fractional shortening, using a small animal ultrasound imaging system (Vevo2100, VisualSonics, Canada). Functional cardiac indices were calculated based on the average of three or more consecutive cardiac cycles. All measurements were performed by investigators blinded to the experimental groups.

Histological analysis

Paraffin-embedded myocardial tissues from the LV were sectioned and stained using Masson's trichrome method. In the stained sections, collagen fibers appeared blue, while muscle fibers were stained red. Images were acquired using a Nikon inverted microscope imaging system (Nikon, Germany), with three to five randomly selected fields captured per sample. The collagen volume fraction (CVF, %) was quantified using Image-Pro-Plus 6.0 software (Media Cybernetics, Rockville, MD, USA).

Quantitative real-time polymerase chain reaction (qRT-PCR) analysis

Total RNA was extracted from myocardial tissues and cultured cells using TRIzol reagent (Invitrogen, Carlsbad, CA, USA) following the manufacturer's instructions. RNA concentration and purity were assessed with a Scandrop100 ultramicro nucleic acid protein analyzer (Germany). Complementary DNA (cDNA) synthesis was carried out using the QuantiTect Reverse Transcription Kit (QIAGEN, Germany). qRT-PCR was conducted on a BIO-RAD CFX96 real-time PCR system (Bio-RAD, Hercules, CA, USA), and gene expression data were processed using qPCRsoft 3.2 software (Analytik Jena). U6 and glyceraldehyde-3-phosphate dehydrogenase (GAPDH) served as internal controls for normalizing miRNA and mRNA expression levels, respectively. Each sample was tested in triplicate, with inter-replicate variability kept below 0.25. Gene expression levels were quantified using the widely accepted ΔΔCt method ($2^{-\Delta\Delta Ct}$). All primers were obtained from Rib Bio Biotech (Guangzhou, China), a specialized biotechnology provider. For reproducibility and transparency, the complete nucleotide sequences of all primers in this study are listed in Table 1.

Isolation, culture, and immunofluorescence identification of CFs

Neonatal Sprague-Dawley rats (0-1 days old) were euthanized by cervical dislocation, with all procedures conducted in accordance with the UK Animal (Scientific Procedures) Act 1,986 under Home Office project license approval. Under sterile conditions, the thoracic cavity was opened to extract the heart, which was then rinsed once in pre-chilled high-glucose Dulbecco's modified Eagle medium (DMEM; Thermo Fisher Scientific, Waltham, MA, USA). Enzymatic digestion was performed using 4 mL of enzyme solution composed of a 1:1 mixture of 0.05% trypsin (Gibco, Billings, MT, USA) and 0.05% type-II collagenase (Life Technologies, Carlsbad, CA, USA), prepared by dissolving 0.02 g of trypsin and 0.02 g of type-II collagenase in 40 mL PBS. The digestion process was carried out in 3-minute intervals for a total of seven to eight cycles. Digestion was halted by adding an equal volume of complete medium. The resulting cell suspension was filtered through a 70 μm mesh and centrifuged at 1200 rpm for 5 minutes. After discarding the supernatant, cells were resuspended in 2 mL of complete medium and centrifuged again under the same conditions. Cells were then seeded onto culture dishes and subjected to a 45-minute differential adhesion step. The supernatant, containing cardiomyocytes, was transferred to a new dish, while 7 mL of high-glucose DMEM supplemented with 10% FBS was added

TABLE 1. The primer sequences for PCR.

Primers	Sequence (5'-3')
U6	F: CGCTTCGGCAGCACATATAC
	R: TTCACGAATTTGCGTGTCATC
miR-17-5p	F: CAAAGTGCTTACAGTGCAGGTA
Collagen I	F: TAAGGGTCCCCAATGGTGAGA
	R: GGGTCCCTCGACTCCTACAT
Collagen III	F: CTGTAACATGGAAACTGGGGAAA
	R: CCATAGCTGAACTGAAAACCACC
α-SMA	F: CCCAGACATCAGGGAGTAATGG
	R: TCTATCGGATACTTCAGCGTCA
GAPDH	F: GAGAAGGCTGGGGCTCAC
	R: TCTATCGGATACTTCAGCGTCA
BNIP3	F: AACTCAGATTGGATATGGGATTGG
	R: AGAGCAGCAGAGATGGAAGG
PINK1	F: ATCCTCCAGCGAAGCCATC
	R: CTACCGCCTGAACTGTTGAAG
Parkin	F: CTCAGACAAGGACACATCAGTAGC
	R: GGCGGTGGTTACATTGGAAGA
Beclin-1	F: ACATCTGGCACAGTGGACAGTTTG
	R: AGCATGGAGCAGCAACACAGTC

α-SMA, alpha-smooth muscle actin; GAPDH, glyceraldehyde 3-phosphate dehydrogenase; BNIP3, BCL2-interacting protein 3; PINK1, PTEN induced putative kinase 1; Beclin-1, autophagy-related protein-1; F, forward; R, reverse; PCR, polymerase chain reaction.

to the original dish containing CFs. Both dishes were incubated at 37 °C with 5% CO_2. For immunofluorescence identification, cells were fixed, followed by permeabilization and blocking. Samples were incubated with anti-vimentin primary antibody (1:100; #5741, Cell Signaling Technology, Danvers, MA, USA) and then with FITC-conjugated goat anti-rabbit IgG secondary antibody (1:100; #ZF-0311, Zhongshan Golden Bridge Biotechnology, Beijing, China). DAPI (#KGA215-50, KeyGen Biotech, Nanjing, China) was used for nuclear staining. Experimental results confirmed that over 95% of the cells were vimentin-positive (refer to Supplementary Figure S1 for staining images). CFs at passages 2-5 and at 70% confluence were selected for transfection.

Cell transfection procedures

miR-17-5p mimics and their corresponding negative control (NC) were purchased from Rib Bio Biotech (Guangzhou, China). The plasmids pcDNA3.1-NC and pcDNA3.1-BNIP3 were obtained from GenePharma (Shanghai, China). Lipofectamine 3000 (L3000015, Invitrogen, Carlsbad, CA, USA) was used for transfection according to the manufacturer's instructions. CFs cultured in six-well plates were transfected when they reached approximately 70% confluence. Transfection complexes containing miR-17-5p mimic, mimic NC, pcDNA3.1-NC, or pcDNA3.1-BNIP3 were prepared according to standard procedures. Following transfection, cells were maintained at 37 °C in a 5% CO_2 incubator for 24 hours. Subsequently, the culture medium was supplemented with angiotensin II (Ang II; 200 nmol/L, HY-13948, MCE), and cells were incubated for an additional 48 hours before harvesting for further analysis.

Cell Counting Kit-8 (CCK-8) proliferation assay

Cell viability was assessed using the CCK-8 assay kit (C0038, Beyotime, Shanghai, China). CFs were plated in 96-well plates at an initial density of 1 x 10^4 cells/well in 100 μL of culture medium. After adding 10 μL of CCK-8 reagent each well, the plates were incubated for 2 hours under standard conditions. Absorbance was measured at 450 nm using a microplate reader, with higher absorbance values indicating greater cell viability and proliferation. Background absorbance from blank wells was subtracted, and cell viability (%) was calculated using the corresponding formula:

$$\text{Viability} = \frac{(A_{sample} - A_{blank})}{(A_{control} - A_{blank})} \times 100$$

Western blot analysis

Cardiac tissue samples and cultured CFs were homogenized and lysed using radioimmunoprecipitation assay buffer (Beyotime, Shanghai, China). Protein concentrations were measured with a bicinchoninic acid protein assay kit (Beyotime, Shanghai, China). Proteins were separated by electrophoresis on 10% sodium dodecyl sulfate-polyacrylamide gels (SDS-PAGE) and transferred to 0.45 μm polyvinylidene fluoride membranes (Beyotime, Shanghai, China). Membranes were blocked for 20 minutes at room temperature using QuickBlock™ Protein-Free Blocking Buffer (Beyotime, Shanghai,

China), followed by overnight incubation at 4 °C with primary antibodies (Abcam, Cambridge, UK).The primary antibodies used were BNIP3 (1:1000, ab109362), alpha-smooth muscle actin (α-SMA, 1:2000, ab124964), Beclin 1 (1:2000, ab207612), and (GAPDH, 1:1000, ab181602). Membranes were then incubated for 2 hours at room temperature with horseradish peroxidase-conjugated goat anti-rabbit IgG (Abcam ab6721; 1:5000). Protein bands were visualized using a chemiluminescent substrate and imaged with the Tanon-5200 chemiluminescence detection system (Tianneng Technology, Shanghai, China).

Dual-luciferase reporter assay

Based on predictions from TargetScan and miRBase, a segment of the BNIP3 3'-UTR containing the predicted miR-17-5p binding site, along with a corresponding mutant (MUT) version, was synthesized and inserted into the pmirGLO luciferase vector (GenePharma, Shanghai, China). Both WT and MUT BNIP3 reporter plasmids were constructed. HEK293T cells (human embryonic kidney 293T line) were co-transfected with either the miR-17-5p mimic or the NC mimic. Luciferase activity was measured using the Dual-Luciferase Reporter Assay System (Promega, Madison, WI, USA), following the manufacturer's instructions.

Intracellular ROS detection

CFs underwent repeated freeze-thaw cycles, followed by centrifugation at 1500 × g for 10 minutes to collect the supernatant. In accordance with the manufacture's protocol, ROS levels were quantified using a rat ROS enzyme-linked immunosorbent assay kit (J23513, Gilide Biotechnology, Wuhan, China). Absorbance (optical density values) was recorded at 450 nm using a SpectraMax L microplate reader (Molecular Devices, Sunnyvale, CA, USA). ROS concentrations were calculated using standard curves, with blank wells serving as zero references.

Intracellular ATP content

Intracellular ATP content was measured using the Enhanced ATP Assay Kit (#S0027, Beyotime, Shanghai, China) in accordance with the manufacturer's instructions. Cells were lysed with ATP lysis buffer, and the lysates were centrifuged at 12,000 × g for 5 minutes at 4 °C to collect the supernatants for ATP measurement. Relative light unit values were recorded using an ultra-sensitive chemiluminescence detection system (Tanon-5200, Tianneng Technology, Shanghai, China). ATP concentrations were calculated from a standard curve.

Statistical analysis

All statistical analyses were performed using GraphPad Prism 8.02 (GraphPad Software Inc., San Diego, CA, USA). Normality of continuous variables was assessed using the Shapiro-Wilk test ($p > 0.05$), confirming the use of parametric tests throughout. Data are expressed as mean ± standard deviation. For comparisons between two groups, independent sample t-test were applied to parametric data. Categorical data were evaluated using the chi-squared test. Comparisons across multiple groups were conducted using one-way

analysis of variance, followed by Bonferroni post-hoc correction. A two-tailed p-value of < 0.05 was considered statistically significant. For experiments involving multiple comparisons (e.g., qPCR or Western blot analyses of multiple targets, echocardiographic data across time points), the false discovery rate was controlled using the Benjamini-Hochberg method, with significance defined as $q < 0.05$. For in vitro assays, three independent biological replicates were conducted, each using CFs derived from distinct neonatal rat litters. Within each replicate, three technical wells per treatment group were averaged. For *in vivo* studies, mice were assigned to sham or AAC groups using block randomization (block size = 4), stratified by baseline body weight, and group allocation was concealed from the investigator performing the assignments.

RESULTS

miR-17-5p deficiency exacerbates cardiac fibrosis and systolic dysfunction by promoting BNIP3 overexpression in vivo

Echocardiography indicated that the AAC group experienced notable LV enlargement (Figure 1a), as reflected by increased LV end-diastolic diameter (Figure 1b) and LV end-systolic diameter (Figure 1c), alongside impaired systolic performance shown by reductions in LV fractional shortening (Figure 1d) and LV ejection fraction (Figure 1e). Additionally, cardiac hypertrophy was observed, evidenced by elevated LV mass (Figure 1f) and an increased heart weight-to-body weight ratio (Figures 1g, h), in comparison to the sham group. Masson staining revealed intact myocardial architecture and minimal interstitial fibrosis in the sham group, whereas the AAC group showed disrupted myofiber organization and excessive collagen accumulation (Figure 1i). The AAC group also displayed a significantly higher CVF value relative to the sham group (Figure 1j). qRT-PCR of cardiac tissue confirmed that miR-17-5p expression was markedly reduced in the AAC group compared to the sham group (Figure 1k). Furthermore, both BNIP3 mRNA levels (Figure 1l) and protein expression (Figures 1m, n) were significantly upregulated in the AAC group versus sham-operated controls.

miR-17-5p overexpression inhibits Ang II-induced CF activation in vitro

CFs treated with Ang II exhibited a significant decline in miR-17-5p levels compared with untreated controls (Figure 2a). To investigate the role of miR-17-5p in cardiac fibrosis, CFs were transfected with either miR-17-5p mimics or a mimic NC. Transfection with the miR-17-5p mimic led to a notable increase in miR-17-5p expression compared with the control group (Figure 2b). CCK-8 assay results indicated that Ang II-treated CFs had significantly higher metabolic activity than untreated cells. However, miR-17-5p mimic transfection significantly reduced CF activity in the Ang II + miR-17-5p mimic group compared to the Ang II group (Figure 2c).
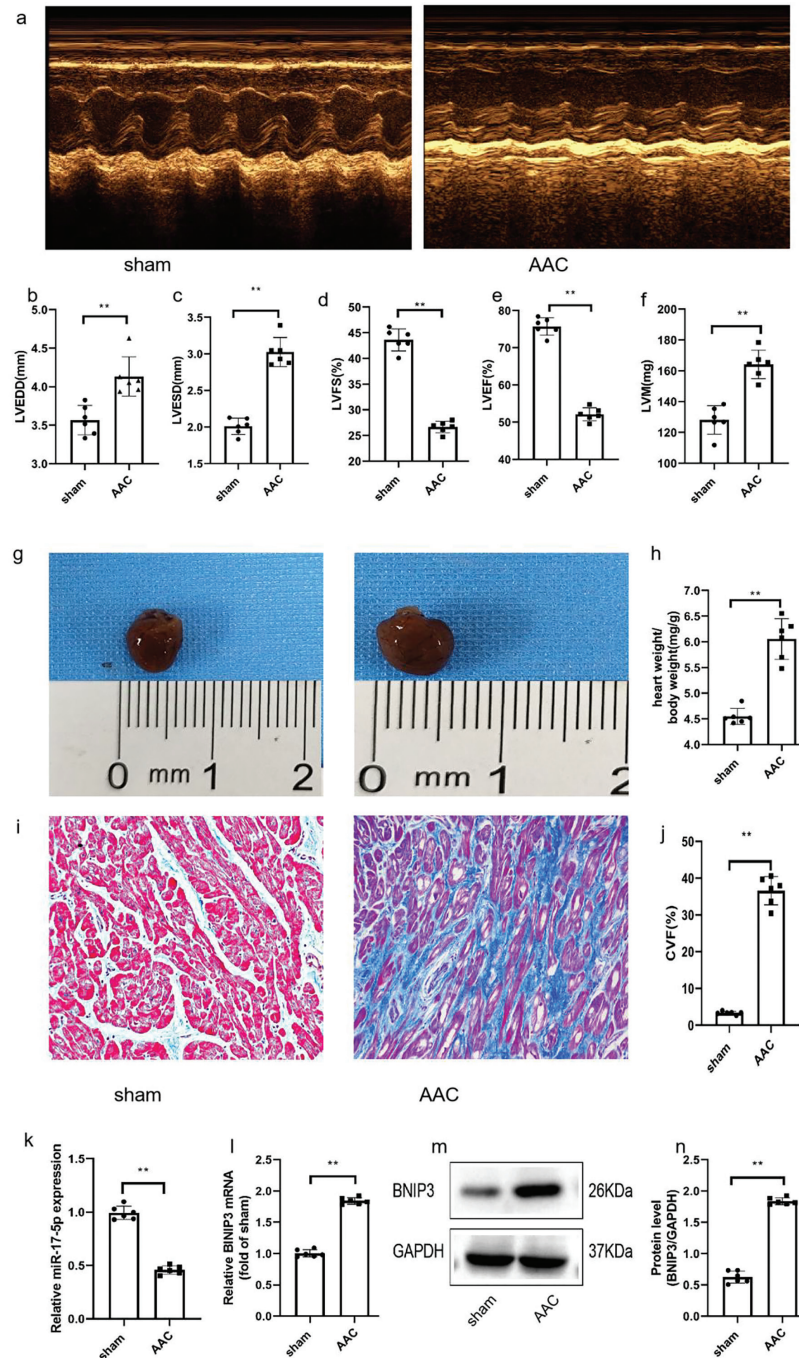
FIG. 1. miR-17-5p deficiency exacerbates cardiac fibrosis and systolic dysfunction via BNIP3 overexpression. (a) M-mode echocardiographic images of mice were measured at 12 weeks after AAC. (b-f). The left ventricular dimensions LVEDD (b), LVESD (c), cardiac function parameters LVFS (d), LVEF (e), and LVM (f) of mice were statistically analyzed 12 weeks post-AAC. (g-h). Representative images of mouse heart gross morphology (g) and statistical analysis of heart weight/body weight ratio (h). (i) Representative images of cardiac interstitial and perivascular fibrosis in murine hearts by Masson staining (× 200). (j) The CVF of myocardial tissue in different groups was statistically analyzed. (k-l). mRNA expression levels of miR-17-5p (k) and BNIP3 (l) were quantified by RT-qPCR in myocardial tissues. (m-n). Representation (m) and statistics (n) of BNIP3 protein relative expression level in myocardial tissue revealed by Western Blot, Bar graphs indicated relative levels of proteins vs. sham control normalized to GAPDH. *$p < 0.05$, **$p < 0.01$, n = 6.

AAC, abdominal aortic constriction; BNIP3, BCL2-interacting protein 3; LVEDD, left ventricular end-diastolic diameter; LVESD, left ventricular end-systolic diameter; LVFS, left ventricular fractional shortening; LVEF, left ventricular ejection fraction; LVM, left ventricular mass; CVF, collagen volume fraction; RT-qPCR, reverse transcription quantitative polymerase chain reaction.

miR-17-5P overexpression inhibits the fibrosis response of Ang II-induced CFs

CFs pretreated with Ang II were transfected with either miR-17-5p mimic or NC. In the absence of Ang II stimulation, qRT-PCR analysis showed no significant differences in the mRNA levels of α-SMA, collagen I, or collagen III between cells transfected with the miR-

17-5p mimic and those with mimic NC. Upon Ang II treatment, there was a marked increase in α-SMA (Figure 3a), collagen I (Figure 3b), and collagen III (Figure 3c) mRNA expression. Importantly, transfection with the miR-17-5p mimic significantly reduced the expression of these profibrotic markers compared to the Ang II + mimic NC group.
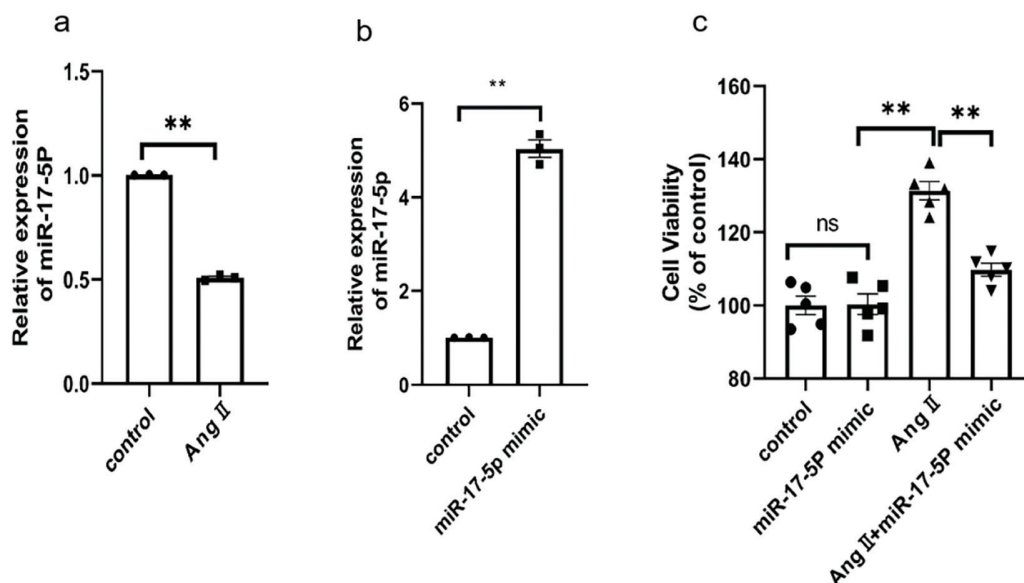

FIG. 2. Relative expression of miR-17-5p and its effect on the cell viability of CFs. (a) miR-17-5p expression levels in control and Ang II group, revealed by RT-qPCR. (b) Comparison of the relative expression levels of miR-17-5p between the control group and the miR-17-5p mimic group. (c) Cell viability of CFs between different treatment groups. **$p < 0.01$, ns means no significance, n ≥ 3.

CFs, cardiac fibroblasts; RT-qPCR, reverse transcription quantitative polymerase chain reaction.
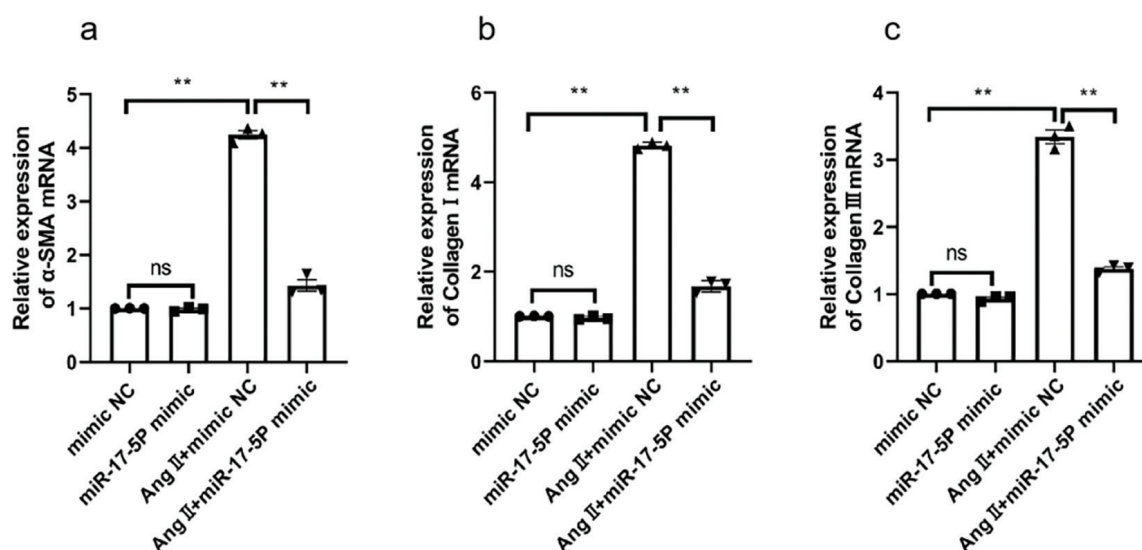

FIG. 3. Effects of differential expression of miR-17-5p on the fibrotic phenotype of CFs stimulated by Ang II. (a-c). Relative expression of α-SMA (a), collagen I (b) and collagen III (c) mRNA in CFs with different *miR-17-5p* gene modifications. **$p < 0.01$, ns means no significance, n = 3.

CFs, cardiac fibroblasts.

BNIP3 is a direct target of miR-17-5p

According to predictions from TargetScan (http://www.targetscan.org), miR-17-5p is expected to bind to the 3'-UTR at positions 363-369 (Figure 4a). The dual-luciferase reporter assay demonstrated reduced luciferase activity in cells co-transfected with the miR-17-5p mimic and the WT BNIP3 3'-UTR vector compared to the WT + mimic NC group (Figure 4b). In contrast, luciferase activity remained unchanged between the MUT + mimic NC and MUT + miR-17-5p mimic groups (Figure 4b). Furthermore, Western blot analysis revealed significantly elevated BNIP3 protein levels in the Ang II-treated group compared to the control group (Figures 4c, d).

miR-17-5p promotes mitochondrial autophagy by upregulating BNIP3 expression in CFs

To investigate whether miR-17-5p targets BNIP3 to modulate mitochondrial function in CFs, we assessed BNIP3 mRNA and protein levels in the pcDNA3.1-NC or pcDNA3.1-BNIP3 groups. The findings revealed significantly elevated BNIP3 mRNA (Figure 5a) and protein expression (Figures 5b, c) in the pcDNA3.1-BNIP3 group compared to the pcDNA3.1-NC group. BNIP3 and PINK1/Parkin are key regulators of mitochondrial autophagy. Ang II was applied to CFs following co-transfection with either miR-17-5p mimic or mimic NC, along with pcDNA3.1-BNIP3. Mitophagy-related markers were examined via Western blot and qRT-PCR. Ang II stimulation notably upregulated both BNIP3 and Beclin-1 at the mRNA and protein levels, while miR-17-5p mimic transfection significantly reduced their expression. Importantly, co-transfection with pcDNA3.1-

BNIP3 counteracted the miR-17-5p-mediated suppression of BNIP3. Although Ang II enhanced PINK1 and Parkin expression in CFs, their levels remained unaffected by either miR-17-5p mimic or pcDNA3.1-BNIP3 transfection (Figures 5d-f).

To further evaluate the impact of miR-17-5p on mitochondrial function, intracellular ATP levels and ROS concentrations were measured in CFs across different experimental setups. Ang II significantly reduced ATP levels and increased intracellular ROS compared to controls. In contrast, miR-17-5p mimic transfection restored ATP content (Figure 5g) and suppressed excessive ROS production (Figure 5h). However, this protective effect was negated by BNIP3 overexpression via pcDNA3.1-BNIP3 transfection.

DISCUSSION

Our results show that miR-17-5p is consistently downregulated in both AAC-induced myocardial fibrosis models and in CFs exposed to Ang II. Mechanistically, suppression of miR-17-5p led to mitochondrial hyperautophagy through the BNIP3/Beclin-1 pathway, resulting in excessive ROS generation, impaired ATP production, disrupted cellular energy metabolism, and activation of a fibrotic phenotype. In contrast, upregulation of miR-17-5p counteracted these pathological changes and attenuated the fibrotic response. These findings identify the miR-17-5p/BNIP3 pathway as a central mechanism underlying myocardial fibrosis by modulating mitochondrial autophagy, and suggests its potential as a therapeutic target for cardiac fibrosis.
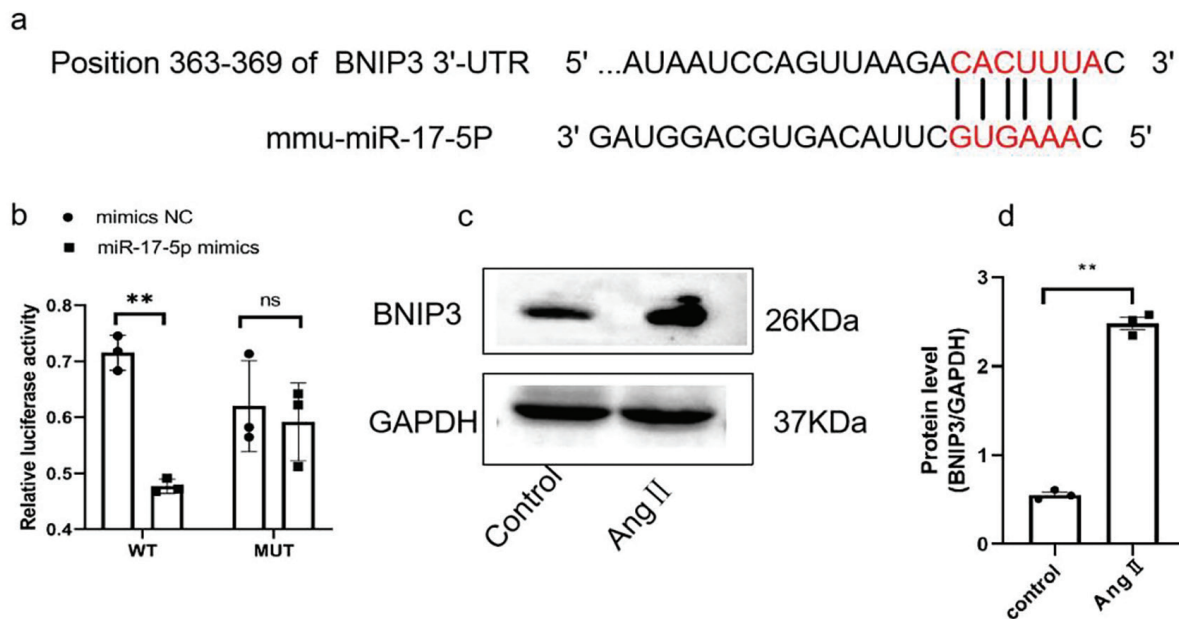

FIG. 4. BINP3 was a direct target of miR-17-5P. (a) The binding site of miR-17-5p and BNIP3 was predicted by TargetScan software. (b) Determination of relative luciferase activity of cells with mimic NC or miR-17-5p mimic and BNIP3-WT or BNIP3-MUT co-transfection by dual-luciferase reporter assay. c-d. Representation (c) and statistics (d) of BNIP3 protein expression in CFs between control and Ang II groups, revealed by Western Blot, and GAPDH was used as the normalization criterion. **$p < 0.01$, ns means no significance, n = 3.

BNIP3, BNIP3, BCL2-interacting protein 3; MUT, mutant; CFs, cardiac fibroblasts; GAPDH, glyceraldehyde-3-phosphate dehydrogenase.
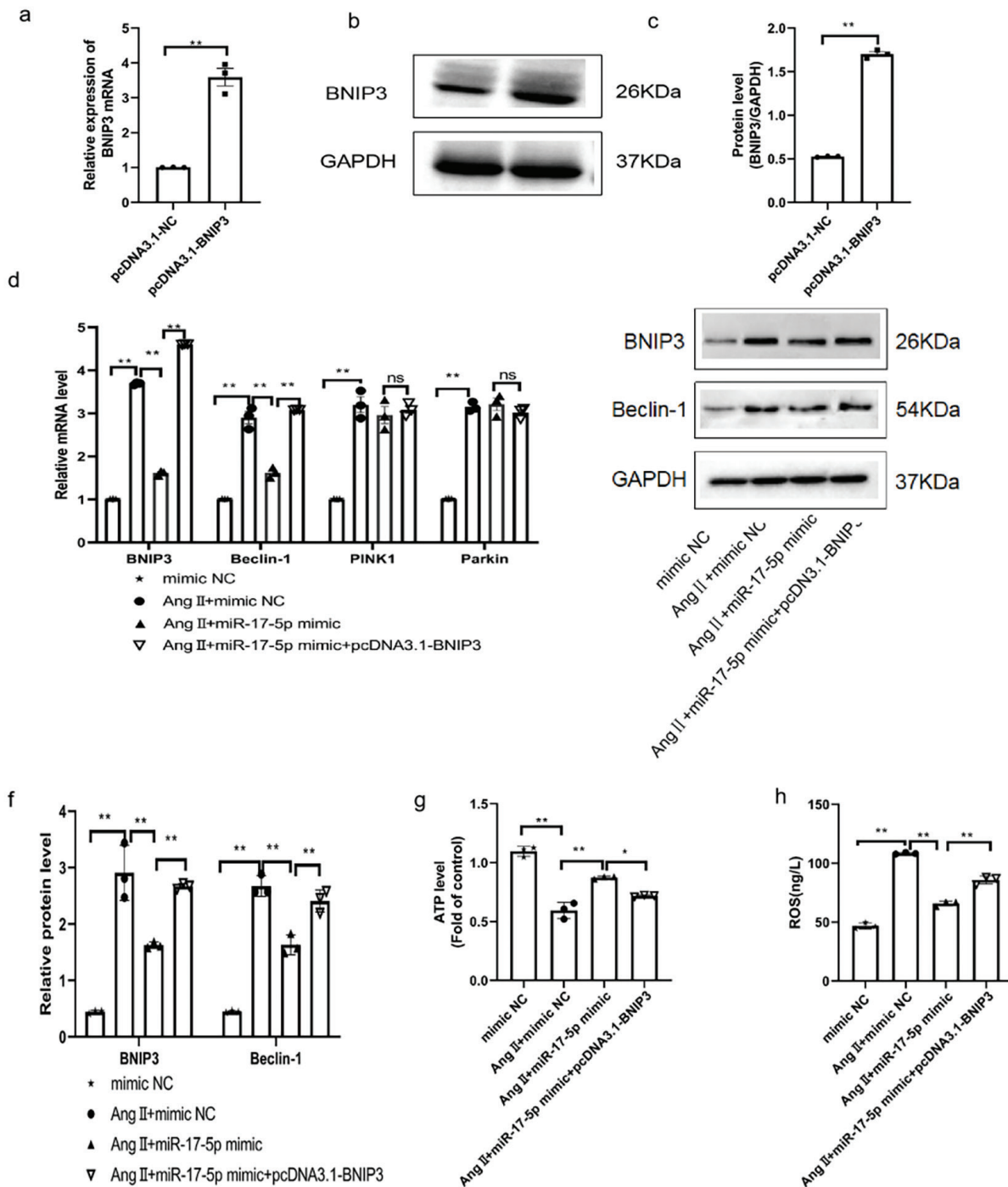
FIG. 5. miR-17-5P regulates mitochondrial homeostasis in CFs by targeting BNIP3. Western blotting was used to detect the protein expression levels of BNIP3 and Beclin-1. The GAPDH level was used for standardized control. (a) The mRNA expression level of BNIP3 in the control and pcDNA3.1-BNIP3 groups was revealed by the RT-qPCR. (b, c). Representation (b) and statistics (c) of BNIP3 protein relative expression level in pcDNA3.1-NC and pcDNA3.1-BNIP3 group revealed by Western Blot. (d) Relative mRNA expression levels of BNIP3, Beclin-1, PINK1, and Parkin were detected by qRT-PCR. e-f. Representation (e) and statistics (f) of BNIP3 and Beclin-1 protein relative expression levels between treatment groups revealed by Western Blot. g-h. Determination of ATP (g) content and ROS (h) levels by ATP assay kit and enzyme linked immunosorbent assay. *$p < 0.05$, **$p < 0.01$, ns means no significance, n = 3.

BNIP3, BCL2-interacting protein 3; CFs, cardiac fibroblasts; GAPDH, glyceraldehyde-3-phosphate dehydrogenase, RT-qPCR, reverse transcription quantitative polymerase chain reaction; ROS, reactive oxygen species; ATP, adenosine triphosphate.

CFs play a pivotal role in the development of myocardial fibrosis. Under pathological stimuli, CFs become activated and produce large amounts of collagen I and III, along with pro-inflammatory mediators, which enhance oxidative stress and autophagy, thereby accelerating fibrotic progression.[18] Consequently, targeting CF activation has emerged as a promising antifibrotic approach. Many miRNAs function are known to act as epigenetic regulators of CF proliferation, activation, and ECM remodeling.[19,20] Previous studies have associated miR-17-5p with the development of atherosclerosis and aortic aneurysms.[21-23] In fibrotic contexts, miR-17-5p has been shown to promote myofibroblast differentiations in oral submucous fibrosis by targeting Smad7[24] and to reduce collagen accumulation in pulmonary fibrosis by suppressing thrombospondin-2.[25] In cardiac remodeling, signal transducer and activator of transcription 3 functions as a key modulator that suppresses myocardial autophagy and influences post-MI remodeling. Our findings align in part with these reports. However, previous studies did not address mitophagy in CFs. This study is the first to demonstrate that miR-17-5p directly targets BNIP3, a critical regulator of mitophagy, linking it to mitochondrial homeostasis in CFs. Moreover, both cellular and animal model evidence confirm that the miR-17-5p/BNIP3 pathways mitigates fibrosis by restoring mitochondrial function, revealing a novel mechanism that expands on earlier research.

Furthermore, miR-17-5p overexpression restores mitochondrial function in CFs. Previous studies have shown that Ang II induces mitochondrial dysfunction by suppressing antioxidant enzyme activity.[26,27] Given that mitochondria are essential for energy metabolism and redox balance, their dysfunction is strongly associated with fibrogenesis. For instance, mitochondrial dysfunction driven by the Wnt/β-catenin/RAS pathway has been linked to renal fibrosis[28], and elevated mitochondrial ROS production contributes to liver fibrosis.[29] Furthermore, miRNAs are increasingly recognized as key regulators of mitochondrial activity. For example, miR-21-5p modulates mitochondrial autophagy and improves mitochondrial network dynamics[30], while overexpression of miR-149-3p and miR-204-5p has been shown to restore mitochondrial function and protect cells from ischemia-induced injury.[31] In this study, miR-17-5p overexpression effectively counteracted Ang II-induced ROS accumulation, restored ATP levels, and suppressed the expression of fibrotic markers in CFs. These results are consistent with the aforementioned studies, indicating that miR-17-5p contributes to the preservation of mitochondrial integrity and the attenuation of fibrosis. Mechanistically, miR-17-5p directly targets BNIP3. BNIP3 initiates mitochondrial autophagy by forming homodimers on the outer mitochondrial membrane.[32] Recent evidence suggests that both insufficient and excessive mitophagy can contribute to the progression of fibrosis.[33] Notably, BNIP3-mediated mitophagy has been implicated in various fibrotic diseases, including renal[13] and pulmonary fibrosis.[34] Functional analyses indicate that Ang II stimulation elevates BNIP3 expression, triggers mitochondrial hyperautophagy, and aggravates pathological changes. These effects induced by Ang II are reversed by miR-17-5p overexpression but negated when BNIP3 is overexpressed, indicating that the antifibrotic action of miR-17-5p is dependent on BNIP3 regulation. These observations are in line with earlier findings on BNIP3's role in promoting apoptosis[35] and the cardiovascular protective properties of nanocurcumin.[36] Additionally, recent studies have identified SCF-

FBXL4 ubiquitin ligase as a negative regulator of mitophagy through the ubiquitin-mediated degradation of BNIP3L and BNIP3[37], offering new mechanistic insights for developing antifibrotic treatments.

This study presents novel experimental evidence supporting the role of miR-17-5p in treating pathological myocardial fibrosis, with implications for clinical translation. Owing to their tissue specificity and functional versatility, miRNAs are considered promising therapeutic agents for various diseases, with several miRNA mimics and inhibitors already undergoing clinical trials.[38] Our findings suggest that enhancing miR-17-5p expression-through gene therapy, small molecule compounds, or exosome-mediated delivery-may represent a viable strategy for treating myocardial fibrosis. Specifically, the study demonstrates that miR-17-5p counters Ang II-induced fibrotic changes, indicating potential for therapeutic application in heart failure secondary to hypertensive cardiomyopathy. Furthermore, miR-17-5p's ability to preserve mitochondrial function and improve energy metabolism suggests broad therapeutic relevance for mitigating myocardial injury, preventing adverse remodeling, and preserving cardiac function.

Interestingly, previous studies have reported roles of miR-17-5p in fibrosis across other tissues: exosome circCDK13 derived from human bone marrow mesenchymal stem cells modulates liver fibrosis via miR-17-5p[39]; miR-17-5p regulates fibrosis in diabetic nephropathy by targeting KIF23[40]; and in pulmonary fibrosis, it binds to thrombospondin 2 to exert its effects.[25] In contrast, this study offers the first evidence that miR-17-5p contributes to myocardial fibrosis by targeting BNIP3 to regulate mitophagy-revealing a distinct mechanism compared to other organs. This unique regulatory axis underscores the novelty of the findings provides a mechanistic basis for targeted interventions in cardiac fibrosis.

In conclusion, this study sheds light on the regulatory function of the miR-17-5p/BNIP3 pathway in myocardial fibrosis. Through both *in vivo* and *in vitro* experiments, we show that miR-17-5p downregulates BNIP3, thereby suppressing Ang II-induced excessive autophagy and preserving mitochondrial integrity, ultimately alleviating pathological myocardial fibrosis. Together, these findings highlight the dual role of mitochondrial autophagy in cardiac fibrosis and suggest new directions for therapeutic development.

REFERENCES

1. Vaduganathan M, Mensah GA, Turco JV, Fuster V, Roth GA. The global burden of cardiovascular diseases and risk: a compass for future health. *J Am Coll Cardiol.* 2022;80:2361-2371. [CrossRef]

2. Tsao CW, Aday AW, Almarzooq ZI, et al. Heart disease and stroke statistics-2022 update: a report from the American Heart Association. Circulation. 2022;145:e153-e639. Erratum in: *Circulation.* 2022;146:e141. [CrossRef]

3. de Boer RA, De Keulenaer G, Bauersachs J, et al. Towards better definition, quantification and treatment of fibrosis in heart failure. A scientific roadmap by the Committee of Translational Research of the Heart Failure Association (HFA) of the European Society of Cardiology. *Eur J Heart Fail.* 2019;21:272-285. [CrossRef]

4. Wang Y, Yu J, Ou C, et al. miRNA-146a-5p inhibits hypoxia-induced myocardial fibrosis through EndMT. *Cardiovasc Toxicol.* 2024;24:133-145. [CrossRef]

5. Wu Y, Zhang S, Gong X, et al. The epigenetic regulators and metabolic changes in ferroptosis-associated cancer progression. *Mol Cancer.* 2020;19:39. [CrossRef]

6. Sygitowicz G, Maciejak-Jastrzebska A, Sitkiewicz D. A review of the molecular mechanisms underlying cardiac fibrosis and atrial fibrillation. *J Clin Med.* 2021;10:4430. [CrossRef]

7. Ning R, Li Y, Du Z, et al. The mitochondria-targeted antioxidant MitoQ attenuated PM(2.5)-induced vascular fibrosis via regulating mitophagy. *Redox Biol.* 2021;46:102113. [CrossRef]

8. Zhu J, Schworer S, Berisa M, et al. Mitochondrial NADP(H) generation is essential for proline biosynthesis. *Science.* 2021;372:968-972. [CrossRef]

9. Niu X, Jiao Z, Wang Z, et al. MiR-17-5p protects neonatal mice from hypoxic-ischemic brain damage by targeting Casp2. *Neurosci Lett.* 2022;772:136475. [CrossRef]

10. Wei Q, Su J, Meng S, et al. MiR-17-5p-engineered sEVs encapsulated in GelMA hydrogel facilitated diabetic wound healing by targeting PTEN and p21. *Adv Sci (Weinh).* 2024;11:e2307761. [CrossRef]

11. Chu Z, Huang Q, Ma K, et al. Novel neutrophil extracellular trap-related mechanisms in diabetic wounds inspire a promising treatment strategy with hypoxia-challenged small extracellular vesicles. *Bioact Mater.* 2023;27:257-270. [CrossRef]

12. Yang C, Yi B, Yang S, et al. VDR restores the expression of PINK1 and BNIP3 in TECs of streptozotocin-induced diabetic mice. *Life Sci Alliance.* 2024;7:e202302474. [CrossRef]

13. Li J, Lin Q, Shao X, et al. HIF1alpha-BNIP3-mediated mitophagy protects against renal fibrosis by decreasing ROS and inhibiting activation of the NLRP3 inflammasome. *Cell Death Dis.* 2023;14:200. [CrossRef]

14. Liu J, Xie Y, Cui Z, et al. Bnip3 interacts with vimentin, an intermediate filament protein, and regulates autophagy of hepatic stellate cells. *Aging (Albany NY).* 2020;13:957-972. [CrossRef]

15. Yu X, Gu P, Huang Z, et al. Reduced expression of BMP3 contributes to the development of pulmonary fibrosis and predicts the unfavorable prognosis in IIP patients. *Oncotarget.* 2017;8:80531-80544. [CrossRef]

16. Chen Y, Jiao D, Liu Y, et al. FBXL4 mutations cause excessive mitophagy via BNIP3/BNIP3L accumulation leading to mitochondrial DNA depletion syndrome. *Cell Death Differ.* 2023;30:2351-2363. [CrossRef]

17. Weinheimer CJ, Kovacs A, Evans S, Matkovich SJ, Barger PM, Mann DL. Load-dependent changes in left ventricular structure and function in a pathophysiologically relevant murine model of reversible heart failure. *Circ Heart Fail.* 2018;11:e004351. [CrossRef]

18. Lendahl U, Muhl L, Betsholtz C. Identification, discrimination and heterogeneity of fibroblasts. *Nat Commun.* 2022;13:3409. [CrossRef]

19. Schoettler FI, Fatehi Hassanabad A, Jadli AS, Patel VB, Fedak PWM. Exploring the role of pericardial miRNAs and exosomes in modulating cardiac fibrosis. *Cardiovasc Pathol.* 2024;73:107671. [CrossRef]

20. Trevelyan CJ, MacCannell ADV, Stewart L, et al. MiR-214-3p regulates Piezo1, lysyl oxidases and mitochondrial function in human cardiac fibroblasts. *Matrix Biol.* 2024;132:34-46. [CrossRef]

21. Wang H, He F, Liang B, et al. p53-dependent lincRNA-p21 protects against proliferation and anti-apoptosis of vascular smooth muscle cells in atherosclerosis by upregulating SIRT7 via MicroRNA-17-5p. *J Cardiovasc Transl Res.* 2021;14:426-440. [CrossRef]

22. Tian Y, Li X, Bai C, Yang Z, Zhang L, Luo J. MiR-17-5p promotes the endothelialization of endothelial progenitor cells to facilitate the vascular repair of aneurysm by regulating PTEN-mediated PI3K/AKT/VEGFA pathway. *Cell Cycle.* 2020;19:3608-3621. [CrossRef]

23. Hu J, Jiang Y, Wu X, et al. Exosomal miR-17-5p from adipose-derived mesenchymal stem cells inhibits abdominal aortic aneurysm by suppressing TXNIP-NLRP3 inflammasome. *Stem Cell Res Ther.* 2022;13:349. [CrossRef]

24. Xie C, Zhong L, Feng H, et al. Exosomal miR-17-5p derived from epithelial cells is involved in aberrant epithelium-fibroblast crosstalk and induces the development of oral submucosal fibrosis. *Int J Oral Sci.* 2024;16:48. [CrossRef]

25. Liu Q, Bi Y, Song S, et al. Exosomal miR-17-5p from human embryonic stem cells prevents pulmonary fibrosis by targeting thrombospondin-2. *Stem Cell Res Ther.* 2023;14:234. [CrossRef]

26. Gibb AA, Lazaropoulos MP, Elrod JW. Myofibroblasts and fibrosis: mitochondrial and metabolic control of cellular differentiation. *Circ Res.* 2020;127:427-447. [CrossRef]

27. Huang G, Cong Z, Wang X, et al. Targeting HSP90 attenuates angiotensin II-induced adventitial remodelling via suppression of mitochondrial fission. *Cardiovasc Res.* 2020;116:1071-1084. [CrossRef]

28. Miao J, Liu J, Niu J, et al. Wnt/beta-catenin/RAS signaling mediates age-related renal fibrosis and is associated with mitochondrial dysfunction. Aging Cell. 2019;18:e13004. Erratum in: *Aging Cell.* 2023 May;22(5):e13816. [CrossRef]

29. Deng Z, Ou H, Ren F, et al. LncRNA SNHG14 promotes OGD/R-induced neuron injury by inducing excessive mitophagy via miR-182-5p/BINP3 axis in HT22 mouse hippocampal neuronal cells. *Biol Res.* 2020;53:38. [CrossRef]

30. Sikora M, Smieszek A, Pielok A, Marycz K. MiR-21-5p regulates the dynamic of mitochondria network and rejuvenates the senile phenotype of bone marrow stromal cells (BMSCs) isolated from osteoporotic SAM/P6 mice. *Stem Cell Res Ther.* 2023;14:54. [CrossRef]

31. Gohel D, Shukla S, Rajan WD, Wojtas B, Kaminska B, Singh R. Altered trafficking of miRNAs at mitochondria modulates mitochondrial functions and cell death in brain ischemia. *Free Radic Biol Med.* 2023;199:26-33. [CrossRef]

32. Bravo-San Pedro JM, Kroemer G, Galluzzi L. Autophagy and mitophagy in cardiovascular disease. *Circ Res.* 2017;120:1812-1824. [CrossRef]

33. Jia H, Song Y, Hua Y, Li K, Li S, Wang Y. Molecular mechanism of aerobic exercise ameliorating myocardial mitochondrial injury in mice with heart failure. *Int J Mol Sci.* 2025;26:2136. [CrossRef]

34. Xie X, Wu X, Zhao D, et al. Fluvoxamine alleviates bleomycin-induced lung fibrosis via regulating the cGAS-STING pathway. *Pharmacol Res.* 2023;187:106577. [CrossRef]

35. Shi RY, Zhu SH, Li V, Gibson SB, Xu XS, Kong JM. BNIP3 interacting with LC3 triggers excessive mitophagy in delayed neuronal death in stroke. *CNS Neurosci Ther.* 2014;20:1045-1055. [CrossRef]

36. Lai TC, Lee CW, Hsu MH, et al. Nanocurcumin reduces high glucose and particulate matter-induced endothelial inflammation: mitochondrial function and involvement of miR-221/222. *Int J Nanomedicine.* 2023;18:7379-7402. [CrossRef]

37. Kulkarni P, Nguyen-Dien GT, Kozul KL, Pagan JK. FBXL4: safeguarding against mitochondrial depletion through suppression of mitophagy. *Autophagy.* 2024;20:1459-1461. [CrossRef]

38. Garreau M, Weidner J, Hamilton R, et al. Chemical modification patterns for microRNA therapeutic mimics: a structure-activity relationship (SAR) case-study on miR-200c. *Nucleic Acids Res.* 2024;52:2792-2807. [CrossRef]

39. Ma J, Li Y, Chen M, et al. hMSCs-derived exosome circCDK13 inhibits liver fibrosis by regulating the expression of MFGE8 through miR-17-5p/KAT2B. *Cell Biol Toxicol.* 2023;39:1-22. [CrossRef]

40. Chen X, Gu L, Cheng X, Xing J, Zhang M. MiR-17-5p downregulation alleviates apoptosis and fibrosis in high glucose-induced human mesangial cells through inactivation of Wnt/beta-catenin signaling by targeting KIF23. *Environ Toxicol.* 2021;36:1702-1712. [CrossRef]